17th October 2014

ITO-ITO Dual-Plate Micro-Gap Electrodes: E and EC' Generator-Collector Processes

Andrew J. Gross* and Frank Marken

Department of Chemistry, University of Bath, Bath BA2 7AY UK

To be submitted to Electroanalysis

(Special Richard G. Compton Issue)

Proofs to A. J. Gross

a.gross@bath.ac.uk

Abstract

Tin-doped indium oxide electrodes are fabricated and employed in a dual-plate microtrench geometry with the inter-electrode gap controlling the mass transport conditions in generator-collector mode. Electrodes are fabricated with 2-50 μm gap sizes and variable trench depths by controlling assembly parameters. Non-ideal behaviour is observed for three aqueous redox systems: $Ru(bpy)_3^{3+/2+}$, 1,1'-ferrocenedimethanol and $Ru(NH_3)_6^{3+/2+}$. Under fast mass transport conditions, the former two systems exhibit slower oxidation features. For $Ru(NH_3)_6^{3+/2+}$, non-steady-state behaviour is observed due to irreversible (EC_{irrev}') consumption of oxygen in the microtrench. A mechanism leading to hydrogen peroxide formation via superoxide in $Ru(NH_3)_6^{2+}$ solution is proposed. Under optimised conditions all three redox systems provide reliable trench depth calibration information.

Keywords: *catalysis, electrochemistry, junction, sensors, superoxide*

1. Introduction

Conditions of fast mass transport are desirable in electroanalysis in order to enhance current signals. A considerable body of work exists on the application of micro-disc [1] and nano-disc [2] electrodes where the rate of mass transport is defined by the disc diameter. Similarly, nano-band electrodes [3] have been developed and hydrodynamic agitation methods [4] have been employed to improve detection limits.

An alternative methodology for enhancing currents can be based on generator-collector feedback processes where two working electrodes are operated in close vicinity [5]. Many types of generator-collector systems have been proposed based on the rotating ring-disc [6], scanning electrochemical microscopy systems [7], coupled microdisc [8] and microband electrodes [9] and interdigitated electrode systems [5b, 10]. In recent years, new examples of generator-collector "gap-electrodes" have appeared including electrochemically grown dual-hemispheres [11], focused ion beam machined nano-gaps in tin-doped indium oxide (ITO) [12], and devices based on electro-migration methods [13]. Especially in the field of nano-gap electrochemistry, new lithographically fabricated devices show great promise [14] and nano-gap sizes small enough to record currents for single molecules [15] have been reported.

The inter-electrode gap, especially for dual-plate devices [16], can be seen as the diffusion layer thickness determining parameter. Halving the inter-electrode gap is therefore predicted to double the resulting mass transport controlled limiting current [17]. In the fast transport domain, observed for nano-gap and small micro-gap sizes, there is therefore the opportunity to explore the mechanism for redox reactions in more detail. Adsorption or desorption phenomena, or the presence of short-lived intermediates, are examples of features which remain difficult to observe with slow mass transport, but are possibly rate limiting under fast mass transport conditions.

In this study three one-electron redox processes, $Ru(bpy)_3^{3+/2+}$ oxidation (equation 1), 1,1'-ferrocenedimethanol oxidation (equation 2), and $Ru(NH_3)_6^{3+/2+}$ reduction (equation 3) are

investigated in terms of their reactivity at ITO electrode surfaces. Currents for all three redox systems are employed to "calibrate" the depth of microtrench electrodes.

$Ru(bpy)_3^{2+}$ (aq) $\rightleftharpoons$ $Ru(bpy)_3^{3+}$ (aq) + e- (1)

$Fc(MeOH)_2$ (aq) $\rightleftharpoons$ $Fc(MeOH)_2^{+}$ (aq) + e- (2)

$Ru(NH_3)_6^{3+}$ (aq) + e- $\rightleftharpoons$ $Ru(NH_3)_6^{2+}$ (aq) (3)

ITO-ITO dual-plate microtrench electrodes (see Figure 1) are fabricated with a range of inter-electrode gap sizes and varying trench depths. The calibration of the trench depth via electrochemical measurement of the mass transport limited current response is compared and different types of behaviour for the three redox systems are observed under conditions of fast mass transport.

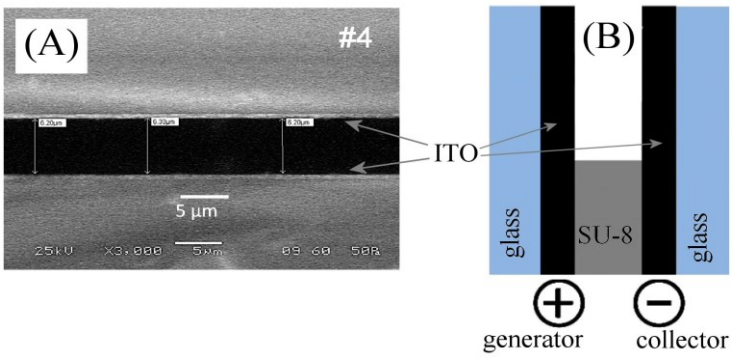

Figure 1. (A) Scanning electron micrograph for an ITO-ITO dual-plate microtrench electrode and (B) schematic drawing showing the generator-collector configuration

Although $Ru(bpy)_3^{3+/2+}$ and $Fc(MeOH)_2$ processes are consistent with a simple "E" mechanism (electron transfer without coupled chemical reaction, Figure 2A), unusual resistive behaviour at the ITO anode requires careful choice of the applied collector potential to avoid artefacts in the mass transport controlled current response. The $Ru(NH_3)_6^{3+/2+}$ reaction is known to be affected by dissolved oxygen [16c]. This is shown here to affect current signals via an EC_{irrev}' [18] mechanism (electron transfer with coupled irreversible chemical step, Figure 2C), where oxygen is consumed irreversibly to produce H_2O_2, leading to higher currents (or a smaller apparent diffusion layer

thickness δ_{app}) and non-steady state features in currents depending on the choice of collector potential. Figure 2b illustrates the alternative EC' case (not observed under the conditions applied here on ITO) involving electron transfer with a follow-up catalytic chemical reaction which in turn enables the original reactant species to be re-generated [18].

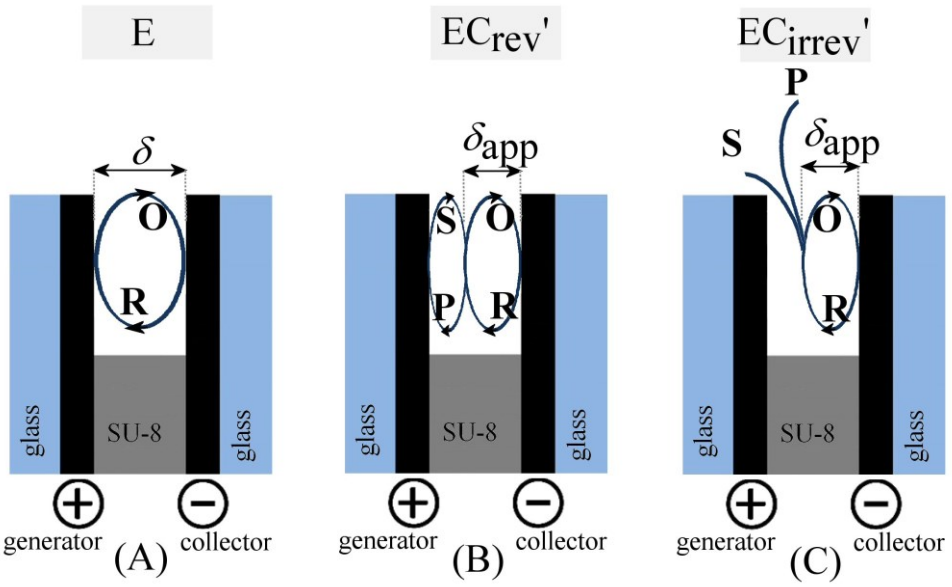

Figure 2. Scheme illustrating microtrench generator-collector feedback reactions: (A) electrochemical "E" loop, (B) "EC_{rev}" double loop and (C) "EC_{irrev}'" one-and-a-half loop, where O/R and S/P correspond to two electrochemical redox systems.

2. Experimental

2.1. Reagents

Sodium chloride (98 %), potassium chloride (≥99 %), mono-sodium phosphate monohydrate (98-102 %), di-sodium hydrogen phosphate heptahydrate (98-102 %), sulphuric acid (≥95-98 %), hydrogen peroxide (30 wt% in water), 1,1-ferrocenedimethanol ($Fc(MeOH)_2$, 98%), cyclopentanone (≥99 %), L-(+)-tartaric acid (≥99.5 %) and oxalic acid dihydrate (≥99.0 %) were purchased from Sigma Aldrich, UK. Hexaammineruthenium(III) chloride ($Ru(NH_3)_6Cl_3$, 99%), Tris(2,2'-bipyridine)ruthenium(II) chloride hexahydrate ($Ru(bpy)_3^{2+}Cl_2$, 98%) and SU-8 2000 series negative photoresists were purchased from Strem Chemicals, Alfa Aesar and Microchem

Corp, respectively. Aqueous solutions were prepared using ultrapure water at 20 °C (resistivity ≥ 18.2 MΩ cm).

2.2. Instrumentation

Electrochemical measurements were performed at 20 ± 2 °C using an SP-300 bipotentiostat (Biologic, France). A four-electrode cell was employed with a Pt wire counter electrode, KCl-saturated calomel electrode (SCE, Radiometer), and the two working electrodes of the microtrench. A WS-650Mz-23NPP (Laurell Technologies) or PWM32 (Headway) spin coater was used to spin photoresist. Scanning electron microscopy (SEM) images were obtained with a JSM-6480LV (JEOL, Japan) and analysed using imageJ 1.48v software. Five independent measurements of inter-electrode gap size were measured per image sampled.

2.3. Procedure: Fabrication of ITO-ITO Micro-Gap Electrodes

Tin-doped indium oxide coated glass (ITO, Image Optics, Basildon, UK) was cut into ≈ 10 mm × 40 mm substrates. A central ≈ 5 mm × 40 mm strip was masked on each substrate using Kapton tape (Farnell, UK) before etching the exposed ITO using a solution of 1 wt.% tartaric acid and 3 wt.% oxalic acid at a temperature of 35°C for 20 min. The substrates were subsequently rinsed with water then placed into a tube furnace for 15 min at 500 °C to remove adventitious impurities and to improve adhesion of photoresist to the surface. After cooling to room temperature, a 10 mm × 5 mm strip of Kapton tape was used to mask one end of each substrate to define a region for electrical contact. The ITO substrates were subsequently spin-coated with a single coat of SU-8 2002, SU-8 2005 or diluted SU-8 2002 (2:1 SU8 2005:cyclopentanone) using a first spin step at 500 rpm (15 sec) and a second spin step in the range 3000-12000 (30 sec) (see Table 1). The Kapton tape was removed and the two substrates were carefully pressed together face-to-face. The substrates were placed on a hot plate pre-heated to 90 °C for 2 min then heated at 160 °C for 5 min. After cooling to room temperature, the end of the ITO-ITO electrode was sliced-off with a diamond cutter (Isomet 1000, Buehler) and the newly exposed end was polished using decreasing grits of SiC abrasive paper (Buehler). The SU-8 layer was partially etched out using piranha solution (5:1 sulphuric acid : hydrogen peroxide; *caution, this is a highly aggressive reagent*) to

form the trench (Figure 1). The etching process was stopped after 5 min (unless otherwise stated) by rinsing with water. Finally, copper tape and silicone sealant were used to isolate the two working electrode contacts.

Table 1. Spin-coating methods used and corresponding inter-electrode gap sizes as determined by SEM.

Sample	Photoresist	Spin programme (two-step)	Measured gap width ± S.D. (μm)	No. of images sampled
1	SU8-2002	i. 500 rpm (15 s) ii. 3000 rpm (30 s)	6.3 ± 0.4	5
2	SU8-2002	i. 500 rpm (15 s) ii. 3000 rpm (30 s)	6.4 ± 1.2	5
3	SU8-2002	i. 500 rpm (15 s) ii. 3000 rpm (30 s)	6.7 ± 0.8	2
4	SU8-2002	i. 500 rpm (15 s) ii. 3000 rpm (30 s)	6.3 ± 0.3	2
5	SU8-2002	i. 500 rpm (15 s) ii. 6000 rpm (30 s)	2.7 ± 0.5	2
6	SU8-2002	i. 500 rpm (15 s) ii. 6000 rpm (30 s)	2.6 ± 0.6	3
7	SU8-2002	i. 500 rpm (15 s) ii. 9000 rpm (30 s)	1.7 ± 0.1	2
8	SU8-2002	i. 500 rpm (15 s) ii. 9000 rpm (30 s)	2.7 ± 0.1	2
9	SU8-2002	i. 500 rpm (15 s) ii. 12000 rpm (30 s)	3.3 ± 0.1	1
10	Dilute SU8-2002	i. 500 rpm (15 s) ii. 3000 rpm (30 s)	4.2 ± 0.3	2
11	Dilute SU8-2002	i. 500 rpm (15 s) ii. 3000 rpm (30 s)	5.5 ± 1.8	2
12	Dilute SU8-2002	i. 500 rpm (15 s) ii. 3000 rpm (30 s)	3.0 ± 0.1	2
13	SU8-2005	i. 500 rpm (15 s) ii. 1000 rpm (30 s)	52.2 ± 1.2	2

3. Results and Discussion

3.1. ITO-ITO Dual-Plate Micro-Gap Voltammetry I.: $Ru(bpy)_3^{3+/2+}$

In order to reliably calibrate the trench depth of an ITO-ITO dual-plate micro-gap electrode, redox systems need to be investigated to explore interferences and complexity associated with interfacial electron transfer under very high mass transport conditions. In micro-gap electrodes the diffusion layer thickness for the "E" mechanism, δ, is defined by the inter-electrode gap and is typically 2-50 μm [13, 16b]. In comparison with typical hydrodynamic methods such as rotating-disc voltammetry, where δ is typically 50-500 μm [6], use here of micro-gap electrodes enables faster mass transport rates by more than an order of magnitude.

The first redox system investigated is the one-electron oxidation of $Ru(bpy)_3^{2+}$ (equation 1). Data in Figure 3 shows that the electron transfer is reversible in nature with the midpoint potential, E_{mid} = 1.05 V vs. SCE, when recorded without feedback (see insets). With the collector electrode potential fixed at 0.5 V vs. SCE, a very drawn out steady-state current response is observed with a

mass transport controlled limiting current, ca. 0.9 μA, close to the solvent window. This estimated limiting current will be employed below (Table 2) to determine the microtrench depth. The drawn out shape of the voltammetric response suggests a non-Butler-Volmer resistive component (ca. 0.5 MΩ) in the rate for interfacial electron transfer for the anodic process. Effects from dissolved oxygen (Figure 3C) or intentionally added H_2O_2 (Figure 3D) remain insignificant for this redox system.

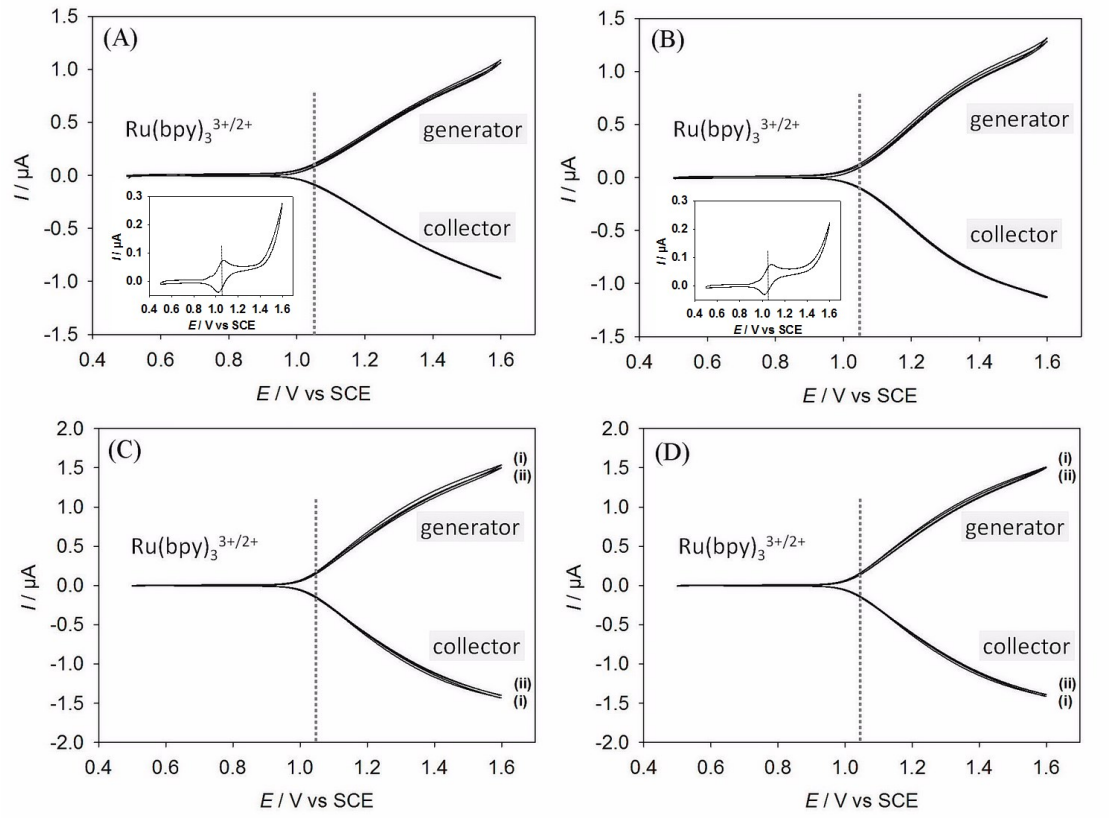

Figure 3. Generator and collector voltammograms obtained at an ITO microtrench (6.3 μm inter-electrode gap) in 1 mM $Ru(bpy)_6^{3+}$ containing 0.1 M KCl as supporting electrolyte with electrode configuration: (A) electrode one and two and (B) electrode two and one as generator and collector, respectively. Insets in (A) and (B) show standard voltammograms recorded at electrode one and electrode two, respectively. Collector potential fixed at 0.5 V vs SCE. (C) (i) before and (ii) after removal of O_2 with collector potential at 0.5 V vs SCE. (D) (i) before and (ii) after addition of 0.5 mM H_2O_2 with collector potential at 0.5 V vs SCE. All scans were recorded at 20 mVs^{-1}.

3.2. ITO-ITO Dual-Plate Micro-Gap Voltammetry II.: 1,1'-Ferrocenedimethanol

Ferrocene derivatives are commonly used calibration systems due to a reliable one-electron mechanism (equation 2) and often fast electron transfer kinetics. Here, 1,1'-ferrocenedimethanol is employed in aqueous 0.1 M KCl. In Figure 4A and 4B insets, typical voltammograms obtained in

the absence of feedback using a standard three-electrode cell are shown. The midpoint potential of E_{mid} = 0.23 V vs. SCE (consistent with literature [19]) suggests that a milder applied oxidation potential will suffice for generator-collector experiments. However, the presence of a secondary response (see Figure 4A inset) at 0.53 V vs. SCE is indicative of limited solubility of the reduced form of $Fc(MeOH)_2$ and possible formation of an anode deposit, impeding rapid oxidation. Under generator-collector feedback conditions, a much higher current (which is shifted to more positive potentials is observed) is observed compared to that obtained in the absence of feedback. The generator and collector signals are broad (sub-Nernstian) and centred on a potential approximately 300 mV more positive when compared to the midpoint potential. As in the case for $Ru(bpy)_3^{2+}$ oxidation, a slow interfacial process for the oxidation (possibly affected by a deposit) appears to affect the voltammetric shape.

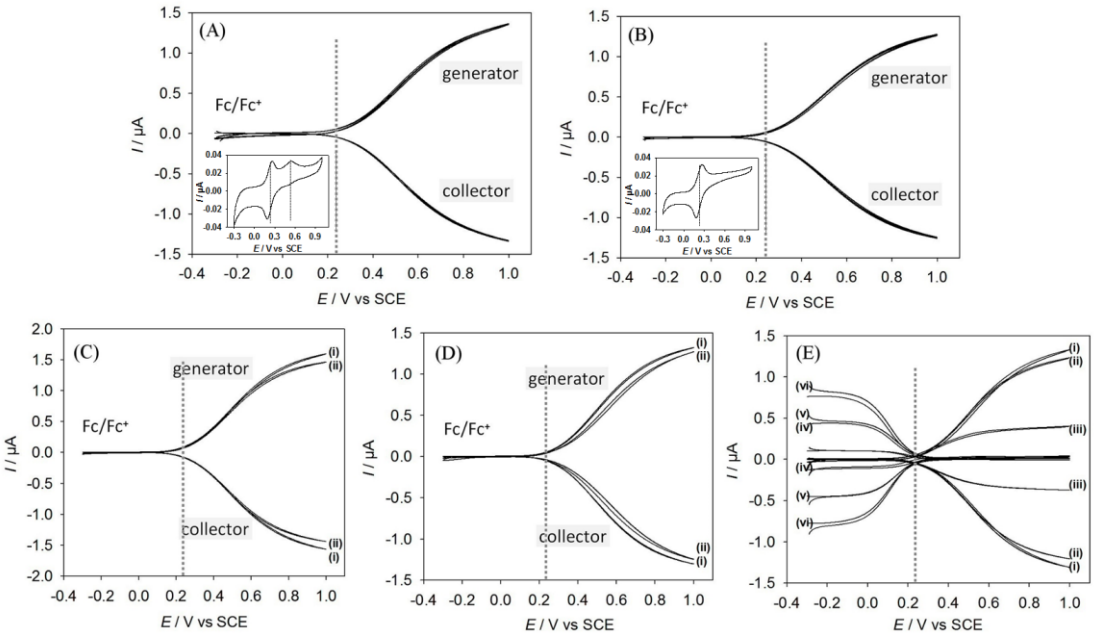

Figure 4. Generator and collector voltammograms obtained at an ITO microtrench (6.3 µm inter-electrode gap) in 0.5 mM $Fc(MeOH)_2$ containing 0.1 M KCl as supporting electrolyte with electrode configuration: (A) electrode one and two and (B) electrode two and one as generator and collector, respectively. Insets in (A) and (B) show standard voltammograms recorded at electrode one and electrode two, respectively. Collector potential fixed at -0.1 V vs SCE. (C) (i) before and (ii) after removal of O_2 with collector potential at -0.1 V vs SCE. (D) (i) before and (ii) after addition of 0.5 mM H_2O_2 with collector potential at -0.1 V vs SCE. (E) with collector potential fixed at (i) -0.3 V, (ii) -0.1 V, (iii) 0.1 V, (iv) 0.3 V, (v) 0.5 and (vi) 0.7 V vs SCE. All scans were recorded at 20 mVs^{-1}.

In Figure 4 the effects of dissolved oxygen (Figure 4C) and addition of 0.5 mM H_2O_2 (Figure 4D) are investigated and this reveals only insignificant changes in steady-state currents. Figure 4E

shows generator-collector voltammograms obtained as a function of the applied collector current. This revealing experiment appears to show two "branches" of redox activity left and right of the midpoint potential (see dashed line). Comparison of the data obtained with the collector potential held at -0.7 V vs SCE (i) with that obtained with the collector potential at 0.7 V vs. SCE (vi) shows that the steady-state current obtained with positive collector potential settings is limited by slow oxidation rather than by mass transport. The "true" mass transport limited steady-state current is obtained as I_{lim} = 1.2 μA (see Table 2).

3.3. ITO-ITO Dual-Plate Micro-Gap Voltammetry III.: $Ru(NH_3)_6^{3+/2+}$

The $Ru(NH_3)_6^{3+/2+}$ redox system is often employed to calibrate micro-gap electrode dimensions and has been used before to investigate the depth of microtrench electrodes [16c, 20]. The one-electron reduction (see equation 3) is associated with fast electron transfer but has also been linked to interferences from dissolved oxygen. Figure 5A and 5B insets show typical voltammetric responses obtained in non-deaerated solution for the reversible Ru(III/II) reduction with a midpoint potential of E_{mid} = -0.19 V vs. SCE [21]. In comparison, generator-collector feedback responses (see Figure 5A and 5B) give considerably higher current responses with steady-state behaviour but with a clear non-steady-state current component. Currents for forward and backward potential sweeps do not re-trace due to reaction of dissolved oxygen (the current diminishes during reduction at negative potentials).

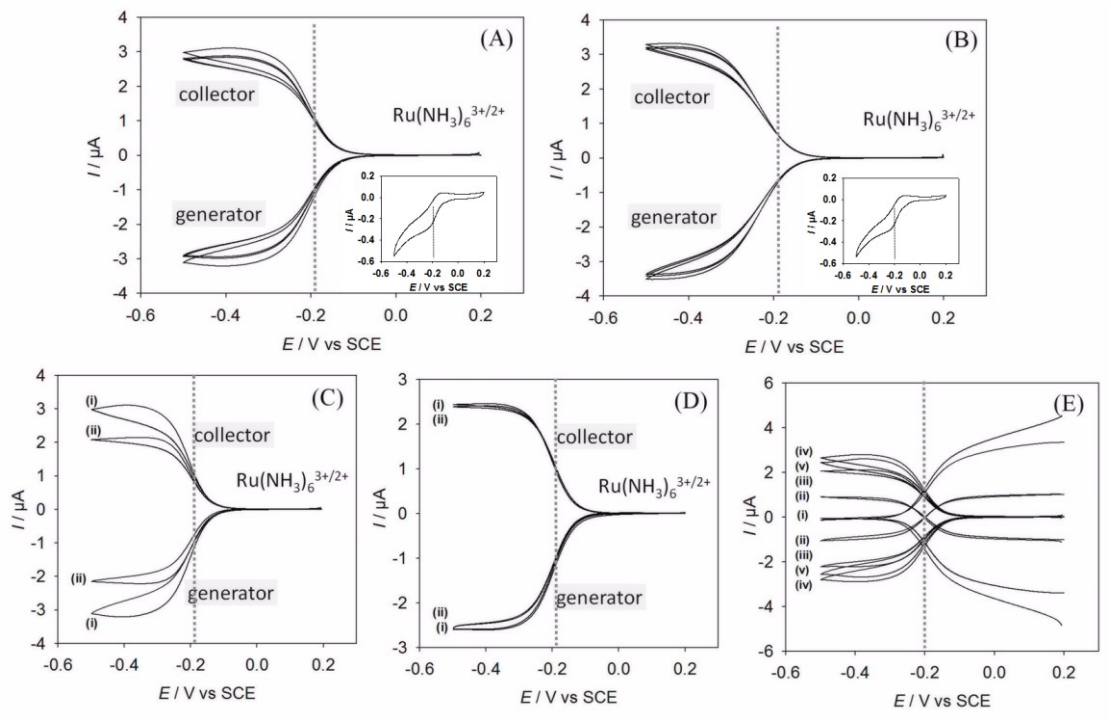

Figure 5. Generator and collector voltammograms obtained at an ITO microtrench (6.3 µm inter-electrode gap) in 1 mM $Ru(NH_3)_6^{3+}$ containing 0.1 M KCl as supporting electrolyte with electrode configuration: (A) electrode one and two and (B) electrode two and one as generator and collector, respectively. Insets in (A) and (B) show standard voltammograms recorded at electrode one and electrode two, respectively. Collector potential fixed at 0.2 V vs SCE. (C) (i) before and (ii) after removal of O_2 with collector potential at 0.2 V vs SCE. (D) (i) before and (ii) after addition of 0.5 mM H_2O_2 with collector potential at 0.2 V vs SCE. (E) with collector potential fixed at (i) -0.4 V, (ii) -0.2 V, (iii) 0.0 V, (iv) 0.2 V, (v) 0.4 vs SCE. All scans were recorded at 20 mVs^{-1}.

The effect of dissolved oxygen is clearly demonstrated in Figure 5C where the limiting current in de-aerated solution (ii) is substantially lower than that obtained under ambient conditions (i). Perhaps surprisingly, intentionally added H_2O_2 (see Figure 5D) does not affect the current, consistent with H_2O_2 being the likely product of mediated oxygen reduction in $Ru(NH_3)_6^{2+}$ under these microtrench conditions. On this basis it can be concluded that $Ru(NH_3)_6^{2+}$ reaction with O_2 produces a superoxide intermediate which then dismutates to give H_2O_2 as the final product (see equations 4 and 5). The process can be classed as EC_{irrev}' (see Figure 2C) where the steady-state characteristic of the current is affected by slow (non-steady-state) diffusion of oxygen into the microtrench.

$$Ru(NH_3)_6^{2+}\,(aq) + O_2\,(aq) \rightleftharpoons Ru(NH_3)_6^{3+}\,(aq) + O_2^{\cdot-}\,(aq) \qquad (4)$$

$$2\,O_2^{\cdot-}\,(aq) + 2\,H^+\,(aq) \longrightarrow O_2\,(aq) + H_2O_2\,(aq) \qquad (5)$$

In order to obtain reliable readings for the mass transport controlled limiting current, the effect of the collector potential was investigated. Figure 5E shows that for $Ru(NH_3)_6^{3+/2+}$ a single well-defined voltammetric wave is obtained independent of the collector potential, consistent with fast interfacial electron transfer. However, the magnitude of the limiting current is clearly affected by the collector potential with negative $E_{collector}$ (see Figure 5Ei) producing the most reliable reading, I_{lim} = ca. 3.1 μA. With the collector potential fixed in the reduction region, continuous removal of dissolved oxygen is more effective and the positive potential region can be explored far enough to avoid limitations by interfacial electron transfer (see $Ru(bpy)_3^{3+/2+}$ and 1,1'-ferrocenedimethanol data). With a reliable mass transport controlled limiting current determined, the trench depth can be estimated by employing the Nernstian diffusion layer model [22] and ignoring edge defects (equation 6).

$$\text{Trench depth} = \frac{I_{lim} \times \delta}{nFDwc} \qquad (6)$$

In this equation the trench depth is obtained from I_{lim}, the mass transport controlled limiting current, δ, the apparent micro-gap width or diffusion layer thickness, n, the number of electrons transferred per molecule diffusing to the electrode surface, F, the Faraday constant, D, the diffusion coefficient (here assumed approximately valid for both oxidised and reduced forms), w, the length of the dual-plate electrode, and c, the bulk concentration of the analyte redox system. Table 2 summarises the depth calibration data.

Table 2. Estimated trench depth values obtained for different aqueous redox systems by using the optimised mass transport limited current with equation 6.

Redox system	Diffusion coefficient ($cm^2\ s^{-1}$)	Gap width ± S.D. (μm)	Estimated I_{lim} (μA)	Estimated trench depth (μm)
1.0 mM $Ru(NH_3)_6^{3+/2+}$ in 0.1 M KCl	9.1×10^{-6} [21]	6.3 ± 0.4	3.1	44 ± 3
0.5 mM $Fc(MeOH)_2^{0/+}$ in 0.1 M KCl	6.4×10^{-6} [11]	6.3 ± 0.4	1.2	49 ± 4
1.0 mM $Ru(bpy)_3^{3+/2+}$ in 0.1 M KCl	2.6×10^{-6} [23]	6.3 ± 0.4	0.9	45 ± 3

It can be seen that generally similar values are obtained (given a level of uncertainty in the concentration of $Fc(MeOH)_2$, the validity of $D_{ox} = D_{red}$, and uncertainty in literature diffusion coefficients). All experiments were performed with the same ITO-ITO dual-plate electrode and

therefore an average value of 46 ± 3 μm (corresponding to an aspect ratio of 7.3) appears reasonable. However, each calibration redox system exhibited complexity and without taking this into consideration the error would be higher.

3.4. ITO-ITO Dual-Plate Micro-Gap Voltammetry IV.: Geometry Modification

The Piranha etch procedure (see Experimental) allows ITO-ITO dual-plate microtrench electrodes to be further modified and the feedback current to be significantly increased by deepening the trench. Deeping of the trench occurs with the removal of increasing amounts of the cured SU-8 spacer layer between the electrodes. This can be demonstrated for different types of ITO-ITO electrodes and as a function of time in Piranha acid. Figure 6A shows data for the reduction of $Ru(NH_3)_6^{3+}$ in 0.1 M KCl using a microtrench electrode with a 3.5 μm gap. When going from a 5 min to 15 min Piranha etch duration, the limiting current clearly increases. Based on equation 6 the current is expected to triple, but non-linearity in particular for small gap electrode systems, is likely to slow down the etch rate for deeper trenches.

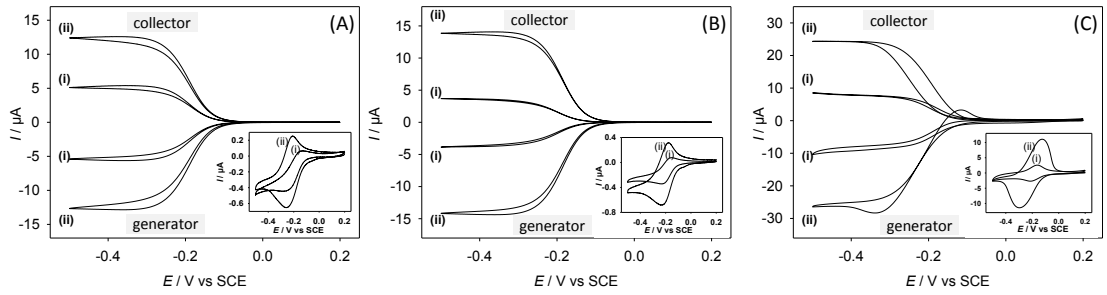

Figure 6. Generator and collector voltammograms obtained at ITO microtrench electrodes with (A) 3.5 μm, (B) 6.7 μm and (C) 22 μm gap size in 1 mM $Ru(NH_3)_6^{3+}$ containing 0.1 M KCl as supporting electrolyte. (i) 5 min piranha etch and (ii) 15 min etch time. Insets show standard voltammograms recorded at electrode one using a three-electrode cell set-up. Collector potential fixed at 0.2 V vs SCE. All scans were recorded at 20 mVs^{-1}.

Figure 6B shows data obtained for a 7 μm gap microtrench electrode, where indeed the limiting current nearly triples when comparing a 5 min etch to a 15 min etch. For etch times longer than 20 mins (data not shown) again a slowing of the etch process is observed. Finally, for a 22 μm gap microtrench (see Figure 6C), the 5 min etch seems to produce a much deeper trench, and when left to etch for 15 min a much higher limiting current is observed. In summary, the formation of ITO-

ITO dual-plate microtrench electrodes can be controlled via simple variation of fabrication parameters (spin coating, type of photoresist and etch conditions) to give reproducible electrodes for applications in electroanalysis.

4. Conclusions

Fabrication of ITO-ITO dual-plate electrodes based on a photoresist spin-coating process followed by thermal annealing and etching is demonstrated. Generator-collector electrode systems are obtained with good reproducibility and good electrochemical properties. Three redox systems are compared; namely, (i) $Ru(bpy)_3^{3+/2+,}$ (ii) 1,1'-ferrocenedimethanol, and (iii) $Ru(NH_3)_6^{3+/2+}$, in order to explore non-ideal features in voltammetric behaviour under conditions of fast mass transport. The voltammetric response for $Ru(bpy)_3^{2+}$ appears shifted into the high potential region (due to interfacial electron transfer rate limitations during oxidation) and therefore mass transport limiting currents can only be estimated. For the oxidation of 1,1'-ferrocenedimethanol impeded oxidation was also observed in the positive potential region, leading to broadening of the voltammetric response. However, with appropriate collector potential settings, reliable limiting current values are obtained. For the $Ru(NH_3)_6^{3+/2+}$ redox system, interference from dissolved oxygen is significant and due to the EC_{irrev}' nature of the mechanism, non-steady-state features appear in the generator-collector voltammograms. In order to overcome this problem either (i) de-aerated solutions must be used or (ii) the collector potential has to be selected negative in a potential region where oxygen is continuously consumed.

Acknowledgements

A.J.G and F.M gratefully acknowledge the Engineering and Physical Sciences Research Council (EP/I028706/1) for financial support.

References

[1] a) A. M. Bond, *Analyst* **1994**, *119*, 1R-21R; b) R. J. Forster, *Chem. Soc. Rev.* **1994**, *23*, 289-297.

[2] a) D. W. M. Arrigan, *Analyst* **2004**, *129*, 1157-1165; b) Y. Shao, M. V. Mirkin, G. Fish, S. Kokotov, D. Palanker, A. Lewis, *Anal. Chem.* **1997**, *69*, 1627-1634.

[3] a) R. Sultana, N. Reza, N. J. Kay, I. Schmueser, A. J. Walton, J. G. Terry, A. R. Mount, N. J. Freeman, *Electrochim. Acta* **2014**, *126*, 98-103; b) S. P. Branagan, N. M. Contento, P. W. Bohn, *J. Am. Chem. Soc.* **2012**, *134*, 8617-8624.

[4] a) I. J. Cutress, F. Marken, R. G. Compton, *Electroanalysis* **2009**, *21*, 113-123; b) S. D. Ahn, P. E. Frith, A. C. Fisher, A. M. Bond, F. Marken, *J. Electroanal. Chem.* **2014**, *722-723*, 78-82.

[5] a) E. O. Barnes, G. E. M. Lewis, S. E. C. Dale, F. Marken, R. G. Compton, *Analyst* **2012**, *137*, 1068-1081; b) O. Niwa, M. Morita, H. Tabei, *Anal. Chem.* **1990**, *62*, 447-452; c) A. J. Bard, J. A. Crayston, G. P. Kittlesen, T. Varco Shea, M. S. Wrighton, *Anal. Chem.* **1986**, *58*, 2321-2331.

[6] W. J. Albery, M. L. Hitchman, *Ring-Disc Electrodes*, Clarendon Press, Oxford, **1971**.

[7] R. D. Martin, P. R. Unwin, *Anal. Chem.* **1998**, *70*, 276-284.

[8] I. J. Cutress, Y. Wang, J. G. Limon-Petersen, S. E. C. Dale, L. Rassaei, F. Marken, R. G. Compton, *J. Electroanal. Chem.* **2011**, *655*, 147-153.

[9] H. Rajantie, D. E. Williams, *Analyst* **2001**, *126*, 86-90.

[10] K. Aoki, M. Morita, O. Niwa, H. Tabei, *J. Electroanal. Chem.* **1988**, *256*, 269-282.

[11] R. W. French, A. M. Collins, F. Marken, *Electroanalysis* **2008**, *20*, 2403-2409.

[12] C. Y. Cummings, J. D. Wadhawan, T. Nakabayashi, M.-a. Haga, L. Rassaei, S. E. C. Dale, S. Bending, M. Pumera, S. C. Parker, F. Marken, *J. Electroanal. Chem.* **2011**, *657*, 196-201.

[13] S. E. C. Dale, Y. Chan, P. C. Bulman Page, E. O. Barnes, R. G. Compton, F. Marken, *Electrophoresis* **2013**, *34*, 1979-1984.

[14] a) L. Rassaei, P. S. Singh, S. G. Lemay, *Anal. Chem.* **2011**, *83*, 3974-3980; b) C. Ma, N. M. Contento, L. R. Gibson, P. W. Bohn, *ACS Nano* **2013**, *7*, 5483-5490.

[15] S. Kang, A. F. Nieuwenhuis, K. Mathwig, D. Mampallil, S. G. Lemay, *ACS Nano* **2013**, *7*, 10931-10937.

[16] a) J. L. Hammond, A. J. Gross, P. Estrela, J. Iniesta, S. J. Green, C. P. Winlove, P. G. Winyard, N. Benjamin, F. Marken, *Anal. Chem.* **2014**, *86*, 6748-6752; b) M. A. Hasnat, A. J. Gross, S. E. C. Dale, E. O. Barnes, R. G. Compton, F. Marken, *Analyst* **2014**, *139*, 569-575; c) S. E. C. Dale, C. E. Hotchen, F. Marken, *Electrochim. Acta* **2013**, *101*, 196-200.

[17] S. E. C. Dale, F. Marken, in *Electrochemistry: Nanoelectrochemistry, Vol. 12* (Eds.: R. G. Compton, J. D. Wadhawan), The Royal Society of Chemistry, Cambridge, **2014**, pp. 132-154.

[18] F. Marken, A. Neudeck, A. M. Bond, in *Electroanalytical Methods: Guide to Experiments and Applications* (Ed.: F. Scholz), Springer, Heidelberg, **2002**, pp. 57-106.

[19] S. J. Stott, R. J. Mortimer, K. J. McKenzie, F. Marken, *Analyst* **2005**, *130*, 358-363.

[20] A. J. Gross, F. Marken, *Electrochem. Commun.* **2014**, *46*, 120-123.

[21] F. Marken, J. C. Eklund, R. G. Compton, *J. Electroanal. Chem.* **1995**, *395*, 335-339.

[22] R. G. Compton, C. E. Banks, in *Understanding Voltammetry*, Imperial College Press, London, **2007**, p. 95.

[23] J. Jin, F. Takahashi, T. Kaneko, T. Nakamura, *Electrochim. Acta* **2010**, *55*, 5532-5537.